

Haksung Moon^a, Je-Hyeong Bahk^b, Fred F. Lange^a

^aMaterials Department, University of California at Santa Barbara, Santa Barbara, California, USA

^bECE Department, University of California at Santa Barbara, Santa Barbara, California, USA

Threshold strength and residual stress analysis of zirconia–alumina laminates

Dedicated to Professor Dr. Wolfgang Pompe on the occasion of his 65th birthday

We dedicate this work to Wolfgang Pompe, a very good friend and a good friend of the Materials Faculty at UCSB where he and his wife, Gisela, shared their lives and fellowship.

Three different zirconia–alumina laminates, AZ50, AZ80, and AZ95, were fabricated via tape-casting thick Zr(3Y)O₂ layers, dip-coating the zirconia tapes in a slurry containing a mixture of zirconia and alumina, stacking and bonding the coated zirconia tapes, followed by densification. Each composite had a different compressive stress by using different mixtures of alumina and zirconia (the number associated with each composite system refers to the volume fraction of alumina in the thin, compressive layers). After densification, the Zr(3Y)O₂ layers were ~ 425 μm thick, and the thin alumina/zirconia layers were 60 ~ 65 μm thick. The threshold strengths, below which the probability of failure is zero, were determined to be 255 ± 8 MPa, 311 ± 7 MPa, and 421 ± 12 MPa for AZ50, AZ80, and AZ95 laminates, respectively. These values are about 60 ~ 70% of those calculated from a previously reported function. The surface and interior stresses were determined using a finite element analysis. The compressive stresses of the outer alumina/zirconia layers were determined using a piezospectroscopy method. The surface stresses for the thick zirconia layers were estimated using an indentation–crack length relation. The piezospectroscopy, analytical and finite element analysis results for the outer compressive layer were in good agreement. But, the finite element analysis showed that the compressive stress component on the surface of the compressive layers was approximately half the value of the biaxial compressive stresses deep within the thin, compressive layers. It appears that the much smaller compressive stresses on the surface of the compressive layers is one important factor that resulted in the lower threshold strength than predicted by the previously developed function used to estimate the threshold strength.

1. Introduction

Previous studies have shown that ceramic laminates containing periodic compressive layers can exhibit a threshold strength, namely, a stress below which the probability of failure is zero. It was shown that the thin compressive layers can stop a propagating crack by reducing the stress intensity factor below the critical value, K_c , at the crack

tip. An increasing applied stress is needed to further extend the crack through the compressive layers in a stable manner. Only when the applied stress is equal to or greater than the threshold strength does the crack extend beyond the compressive layers to produce catastrophic failure. The fundamentals of residual stress, edge cracking and ceramic laminates that exhibit a threshold strength were previously reported in [1–4].

The threshold strength of the ceramic laminates, σ_{thr} , was analytically determined as

$$\sigma_{thr} = \frac{K_c}{\sqrt{\pi \frac{t_2}{2} \left(1 + \frac{2t_1}{t_2}\right)}} + \sigma_c \left[1 - \left(1 + \frac{t_1}{t_2}\right) \frac{2}{\pi} \sin^{-1} \left(\frac{1}{1 + \frac{2t_1}{t_2}} \right) \right] \quad (1)$$

where K_c is the critical stress intensity factor of the thin compressive layer material, t_1 and t_2 are the thicknesses of the thin and thick layers, and σ_c is the residual compressive stress [1].

Different methods have been used to produce and alter the compressive stress in the thin layers. Rao et al. [1] and Moon et al. [2] used an alumina–mullite laminate system in which the differential thermal expansion of the two materials was used to produce the compressive stresses in the thinner laminate. In both studies, the thin layers were composed of different mixtures of alumina and mullite to change the magnitude of the compressive stress. The thicker layers were composed of alumina containing 0.05 volume fraction of Zr(3Y)O₂ to control grain size. Pontin et al. [5] studied the alumina–unstabilized zirconia laminate system. Mixtures of alumina and zirconia were used to produce the thin compressive layers. Alumina containing 0.05 volume fraction of Zr(3Y)O₂ was used for the thick, tensile layers. In this case, the compressive stress arose during cooling and concurrently with the tetragonal to monoclinic zirconia phase transformation. Fillery et al. [6] used an ion exchange technique that produced surface compressive stresses in the surface of glass plates. The plates were bonded together to form glass laminates that have a threshold strength due to the compressive stresses at and near the interfaces between the bonded glass plates.

Zirconia–alumina laminates were fabricated for the present study. The thin, periodic layers were composed of a mixture of alumina and zirconia ($\text{Zr}(3\text{Y})\text{O}_2$, 3 mol.% yttria stabilized zirconia). Different mixtures were used to produce different compressive stresses, relative to the thicker layers with $\text{Zr}(3\text{Y})\text{O}_2$, a transformation toughened material known for its high strength.

Residual stresses on the surface of a laminar composite are very different from the interior stresses, which are biaxial. The surface stresses are tri-axial, with both tensile and compressive components. For example, there is a highly localized surface tensile stress component, equal to the absolute magnitude of the interior biaxial compressive stress, on the surface of the compressive layers; it diminishes to zero when the distance from the surface equals the layer thickness [4]. Because the tensile stresses are highly localized to the surface region, crack extension due to these stresses will only occur when the strain energy released is equal to or greater than the energy absorbed by the extending crack. Thus, much like other phenomena associated with highly localized stress fields (inclusions, thin films, contact stresses, etc), the extension of a surface edge crack along the center of the compressive layer will only occur when the thickness of the compressive layer is greater than a critical value. In general, this surface crack, known as an edge crack, will only extend to a depth approximately equal to the layer thickness.

The main objective of this report is to evaluate the threshold strength of a series of zirconia–alumina laminates, and to determine and compare the surface and interior stress states using several available methods including finite element analysis (FEA), piezospectroscopy, and an analysis of an indentation crack. The effect of surface stresses on the threshold strength will also be discussed.

2. Experimental procedures

2.1. Specimen preparation

Zirconia containing 3 mol.% Y_2O_3 (TZ-3YS, $d_{50} = 0.4 \mu\text{m}$, Tosho, Japan) and alumina (AKP-30, $d_{50} = 0.4 \mu\text{m}$, Sumitomo, Japan) powders were used. Aqueous slurries were prepared using deionized water, the ceramic powders, and a dispersant (Duramax D-3005, Rohm and Haas, Philadelphia, PA). The thick zirconia layers were formed by tape casting. The aqueous tape casting slurry was formulated with 28 vol.% of the zirconia powder and 3.08 wt.% of the dispersant, relative to the powder. The thin layers were formed by dip coating the thick, zirconia tapes into an aqueous slurry containing 20 vol.% of the mixed powders and 3.08 wt.% of the dispersant, relative to the powder.

The slurries were ultra-sonicated (W-380 Sonicator, heat Systems-Ultrasonics, Inc., Farmingdale, NY) for 30 min and then attrition-milled for 1.5 h. Milled slurries were further rolled in plastic containers for at least 12 h. For tape casting and dip coating, an aqueous emulsion binder (Duramax B-1000, Rohm and Haas, Philadelphia, PA) was added at a concentration 20 wt.% and 10 wt.%, respectively, relative to the amount of powder in the slurry. Slurries were filtered through a $38 \mu\text{m}$ mesh screen before both tape casting and dip coating.

The laminates were fabricated to contain five thick zirconia ($\text{Zr}(3\text{Y})\text{O}_2$) layers and six zirconia–alumina, thin

layers. Three different laminates composites were fabricated with three different zirconia–alumina thin layers that sandwiched the thick zirconia layers. Zirconia tapes, 240 to $260 \mu\text{m}$ thick, were made using a tape casting machine (TTC-1000, Richard E. Mistler, Inc., Morrisville, PA) that was equipped with a double doctor blade assembly and a silicone-coated Mylar™ film carrier. Dried tapes were cut into rectangular sheets with the approximate dimensions of $38 \text{ mm} \times 10 \text{ mm}$. Three zirconia sheets were stacked together and pressed at 60 MPa at room temperature to form the thick zirconia layers. These zirconia tapes were then dip coated at 4.3 mm s^{-1} using one of three different mixed alumina–zirconia slurries to make the three different laminates. These laminates were named AZ95, AZ80, and AZ50 where the numbers are the volume percentages of the alumina in the alumina–zirconia mixture used to form the thin compressive layers. With the slurries and dipping condition cited above, each time a zirconia tape was dip coated, a thin layer with a thickness of 20 to $25 \mu\text{m}$ was formed after densification. Thicker compressive layers, e.g. $60 \sim 65 \mu\text{m}$, required multiple dip coatings. The multi-layered composites were formed by stacking five dip coated tapes together and warm pressing with 60 MPa pressure at 70°C (Laboratory Press Model M, CARVER, WI). The laminates were densified at 1600°C for 2 h after the binder was removed by slowly heating between 200 to 600°C at 1 K min^{-1} . The dense laminate plates were diamond cut and surface ground to form bar specimens. A lateral face on each bar was polished to optically observe the surface where the layers terminated.

2.2. Strength measurement and fracture analysis

To determine the threshold strength, cracks with increasing size were introduced into the center of the central thick layer of different bar specimens with increasing load applied to a Vickers indenter. The lengths of the cracks were determined using an optical microscope (Model Eclipse ME600P, Nikon, Tokyo, Japan). Four point flexural bending tests were performed with a screw-driven mechanical testing machine under displacement control (Model 8562, Instron Systems, Canton, MA; cross-head speed = 0.01 mm min^{-1} , fixture spans = 13 and 30 mm). The failure stress was determined using

$$\sigma_f = \frac{3P_f(s_o - s_i)}{2bh^2} \quad (2)$$

where P_f is the failure load, s_o and s_i are the outer and inner spans, b is the specimen width, and h is the specimen height. The fracture surfaces were observed using both an optical microscope and a scanning electron microscope (SEM) (Model XL40 Sirion, FEI USA, Hillsboro, Oregon). The flexural test configuration is shown schematically in Fig. 2.

2.3. Residual stress measurements

Residual stresses were determined using four different methods: a piezospectroscopy method, FEA, an analytical calculation, and an indentation method.

The piezospectroscopy method was used to measure the residual stresses in the out-most thin compressive layers

Table 1. Material properties used for FEA calculation [3, 8]. $\Delta T = 1200^\circ\text{C}$ [9].

Thin Layer	Poisson's Ratio, ν	Thermal Expansion Coefficient, α ($\times 10^{-6}\text{K}^{-1}$)	Elastic Modulus, E (GPa)
AZ50	0.27	9.67	292
AZ80	0.24	8.82	352
AZ95	0.23	8.43	387
Thick Zirconia Layer	0.32	11.35	205

that contained a mixture of alumina and zirconia. The piezospectroscopy method, pioneered by Clarke [7], examines the stress induced shift of the fluorescence spectra produced by Cr^{3+} impurities in the alumina grains [7]. The residual (and/or applied) stress within the alumina will shift the specific peak position designated R_2 such that the stress in the material can be determined. The residual stress within the alumina grains is produced by two effects. The first effect arises because the thin layers containing the alumina also contain a fraction of zirconia that forms a percolating network with a greater thermal expansion coefficient. The second effect is produced when the mixed alumina/zirconia layers are laminated with the thicker zirconia layers, which also induces compressive stresses in the alumina during cooling. It is the stresses due to the second effect that are important to the current work. Thus, in order to determine the stresses due to the lamination of the materials forming the thin and thick layers, the residual stresses caused by the first effect had to be determined using specimens containing the mixed materials that were not laminated with the thick zirconia layers. These specimens were prepared by tape casting the same slurries used for dip-coating and densified as described above. Spectra were observed for both the un-laminated mixed alumina/zirconia specimens and the out-most thin compressive surface layers of the three different laminate systems. The change in the stress within the alumina between the un-laminated and laminated specimens was used to determine the stress in the compressive layers.

FEA was performed using the ANSYS finite element analysis software (JLR, Engineering Solutions Co.) to evaluate residual stresses in the laminates. All the required material properties were found in the literature [3, 8] and they are reported in Table 1. For both the FEA and the analytical calculations, it was assumed that the mismatch strains do not initiate during cooling from very high temperature until the composite is cooled to 1225°C [9], since it is well known that $\text{Zr}(3\text{Y})\text{O}_2$ is nearly superplastic at 1250°C , and very superplastic at 1400°C [10]. Thus, it was assumed that rapid creep would dissipate residual stresses above 1225°C .

Interior stress states can be analytically calculated using the equation given by

$$\sigma_1 = \sigma_c = \varepsilon_r E'_1 \left(1 + \frac{t_1 E'_1}{t_2 E'_2} \right)^{-1} \quad \text{and} \quad \sigma_2 = -\sigma_1 \frac{t_1}{t_2} \quad (3)$$

where σ_1 is the biaxial compressive stress in the thin compressive layers, σ_2 is the biaxial tensile stress in the thick tensile layers, $E'_i = E_i/(1-\nu_i)$, E is the Young's modulus, ν is the Poisson's ratio, and t_1 and t_2 are the thickness of the compressive and tensile (thicker) layers, respectively. ε_r is biaxial mismatch strain due to the thermal expansion mis-

match between thick and thin layers, and it is given by

$$\varepsilon_r = \int_{T_f}^{T_i} (\alpha_1 - \alpha_2) dT \quad (4)$$

where T_i (1225°C) and T_f (25°C) are the initial and final temperatures during cooling, and α_1 and α_2 are the coefficient of thermal expansion of the two materials.

Lastly, residual stresses determinations were carried out with the indentation method for the thick tensile layer on the polished surface. The critical stress intensity factor, K_c , can be determined with the indentation method by using the equation

$$K_c = \chi_r P/c_0^{3/2} = \zeta (E/H)^{1/2} (P/c_0^{3/2}) \quad (5)$$

where K_c is the fracture toughness, χ is a constant which depends on the ratio of elastic modulus (E) to hardness (H), P is the applied load for indentation, $2c_0$ is the crack length, E is the elastic modulus, and H (or HV) is the Vickers hardness given by [11], $HV = 1.854 \frac{P}{d^2}$ (d is the length of the diagonal of the indentation). ζ is a material-independent constant for radial cracks produced with the Vickers indenter: a value of 0.016 was chosen [12].

The residual stresses will alter the crack size produced by the indenter itself. However, K_c is a material property, which is not altered by the residual stresses, therefore a second term, that includes the residual stress, must be added to the Eq. (5) [13].

$$K_c = \chi_r \frac{P}{c^{3/2}} + \sigma_r \Phi c^{1/2} \quad (6)$$

where σ_r is the residual stress, $2c$ is the new crack length under the residual stress, and Φ is a constant chosen to be $\sqrt{\pi}$ [13]. By rearranging Eq. (6), the value of the residual stress can be calculated by

$$\sigma_r = \left[K_c - \chi_r \frac{P}{c^{3/2}} \right] / (\Phi c^{1/2}) \quad (7)$$

Using this method, residual stresses were measured with at least five indentation cracks introduced into the center thick layer of the laminates. Crack lengths were measured with an optical microscope (Model Eclipse ME600P, Nikon, Japan).

3. Results

Figure 1 shows a typical optical micrograph of an AZ95 ceramic laminate, clearly illustrating the edge crack shown as a dark line along the center line of the thin, compressive layer. All of the AZ80 and AZ95 specimens contained edge cracks similar to that shown in Fig. 1, whereas the AZ50

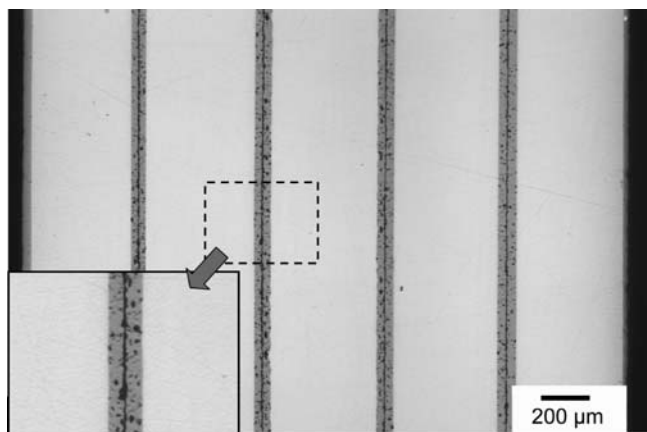


Fig. 1. Optical micrograph showing the surface of an AZ95 laminate. Edge cracks can be observed long the center of each thin, compressive layer. Black dots are grain pull-outs that occurred during surface preparation due to the large tensile stress on the surface of thin layers. A similar observation was made for all AZ80 specimens, whereas AZ50 specimens did not contain edge cracks.

specimens did not exhibit edge cracking. Higher magnification SEM observations (not illustrated) clearly showed that the interfaces between thin and thick layers were well bonded, i.e., no pores were observed, and the zirconia phase in the two layers appeared to ‘blend’ together without a change in grain size. The alumina phase, with a lower Z contrast, defined the demarcation between the thick and thin layers. The thick layers were $\sim 425 \mu\text{m}$ thick, and the thin layers had a thickness of $60 \sim 65 \mu\text{m}$, whereas the out-most thin, compressive layers where $\sim 45 \mu\text{m}$ thick.

3.1. Strength measurements and fracture observations

Figure 2 reports the strength vs. the size of the cracks introduced with the Vickers indenter. Each point represents the strength of a single specimen. Monolith specimens exhibit a strength vs. crack relationship suggested by Griffith, namely, the strength is inversely proportional to square root of crack size. Laminate bars containing thin compressive layers exhibited a threshold strength when the size of the

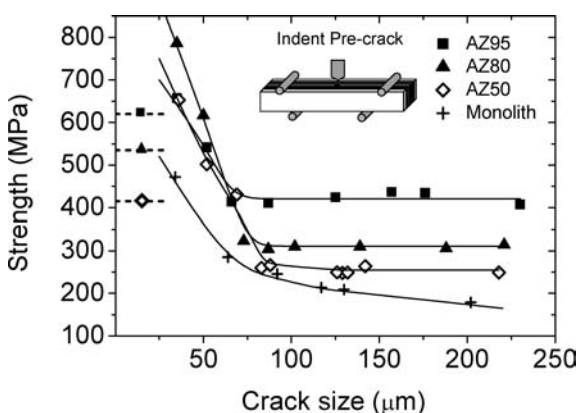


Fig. 2. Plot showing threshold strengths of three laminates (AZ50, AZ80, AZ95) and a monolith. Each of the different laminates exhibits a threshold strength when the pre-crack size, produced by a Vickers indenter, is $>80 \mu\text{m}$. The experimentally measured threshold strengths for AZ50, AZ80, and AZ95 laminates are $255 \pm 8 \text{ MPa}$, $311 \pm 7 \text{ MPa}$, and $421 \pm 12 \text{ MPa}$, respectively. The dotted-partial lines on the left side represent the threshold strengths calculated using Eq. (1). They are 415 MPa , 535 MPa , and 620 MPa , respectively.

crack was greater than $\sim 80 \mu\text{m}$. As shown, the threshold strengths of the AZ50, AZ80, and AZ95 laminates are $255 \pm 8 \text{ MPa}$, $311 \pm 7 \text{ MPa}$, and $421 \pm 12 \text{ MPa}$, respectively. As expected, larger volume fractions of alumina in the thin compressive layers are expected to produce a greater compressive stress, and thus, a larger threshold strength consistent with Eq. (1).

Figures 3–5 illustrate typical fracture surfaces for AZ50, AZ80, and AZ95 laminar specimens, respectively. The fractured surfaces were gold coated and the micrographs were recorded with an optical microscope. Brighter areas of the micrographs are produced by the greater reflectivity of the smoother, initial crack that propagated from the surface crack produced by the indenter, which was arrested by the adjacent thin compressive layers before catastrophic

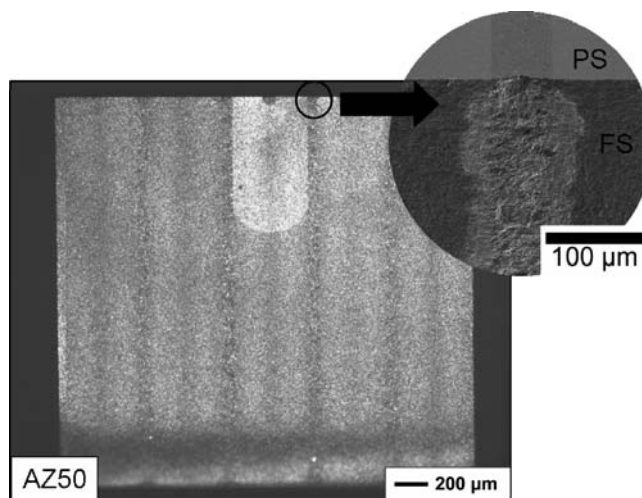


Fig. 3. An optical micrograph of an AZ50 specimen showing the size and shape of the crack arrested by the first two compressive layers it encounters during stressing (bright portion at the center layer). The round insert shows that the crack propagated across the compressive layers without producing a step, indicating that bifurcation did not occur. FS stands for fractured surface and PS stands for polished surface.

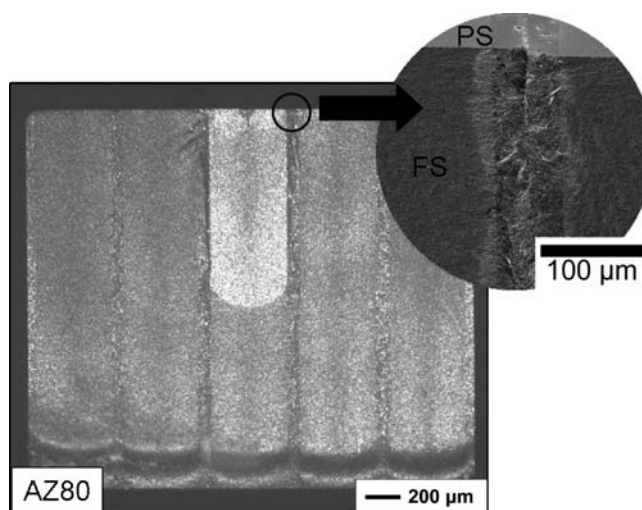


Fig. 4. An optical micrograph of an AZ80 specimen showing the size and shape of the crack arrested by the first two compressive layers it encounters during stressing (bright portion at the center layer). The round insert shows that the crack propagated across the compressive layers and produced a step, indicating that bifurcation did occur. FS stands for fractured surface and PS stands for polished surface.

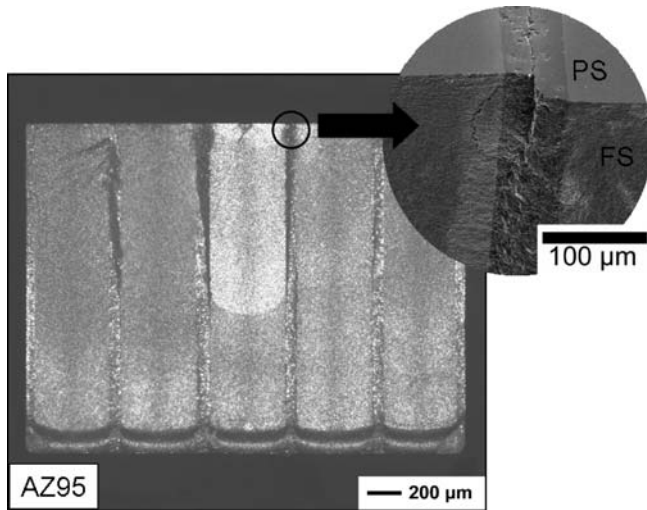


Fig. 5. An optical micrograph of an AZ95 specimen showing the size and shape of the crack arrested by the first two compressive layers it encounters during stressing (bright portion at the center layer). The round insert shows that the crack propagated across the compressive layers and produced a step, indicating that bifurcation did occur. FS stands for fractured surface and PS stands for polished surface.

failure. Specifically, the area of stable crack growth is brighter than that of catastrophic crack growth area because the stable crack growth produced a smoother surface. When catastrophic fracture occurs, the stress intensity factor at the crack tip exceeds both K_c and K_b ($K_I > K_b > K_c$); K_b is the stress intensity factor where crack branching occurs, producing a very rough fracture surface [14]. In all cases, the arrested crack extends from the tensile surface to arrest near the neutral axis of the flexural specimen. As shown, the arrested crack in the AZ95 laminate specimens extended further than that of the AZ80 specimens; the AZ50 specimens had the smallest arrested crack size. These observations suggest that a much larger external stress is needed for an arrested crack to transverse the thin compressive layer of AZ95, which corresponds to the threshold strength reported in Fig. 2.

Cracks were observed to propagate straight through the compressive layer for the AZ50 laminate (see Fig. 3). For the AZ80 and AZ95 laminates, the cracks were deflected when they traversed the thin compressive layers (note larger deflection for AZ95 specimen). Crack bifurcation was observed for the fractured AZ80 and AZ95 specimens. This bifurcation phenomenon is commonly observed when the compressive stresses in the thin layer produce an edge crack, and it is responsible for crack deflection when the crack extends across the compressive layer as noted in Figs. 4 and 5 [1, 3].

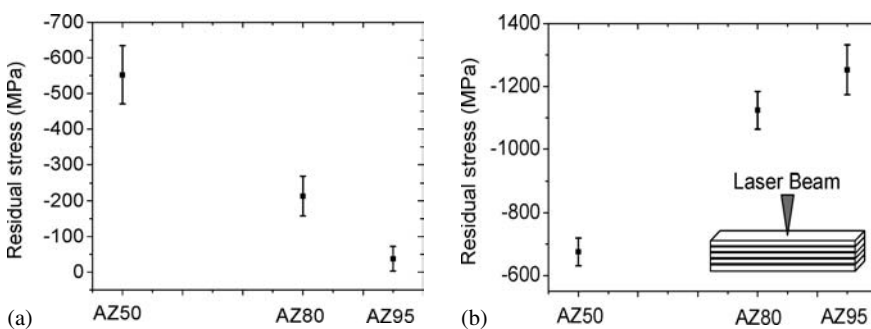


Fig. 6. Piezospectroscopy stress results. (a) The residual stresses for the mixed alumina–zirconia material used to form the laminar composites. Compressive stresses arise in the alumina grains due to the presence of the zirconia grains. Note that the compressive stress that the alumina grain has decreases with the decreasing zirconia content in the two phase mixture. (b) Residual stresses at out-most thin compressive layers within the laminates. Note that the compressive stress in the outer most compressive layer increases with increasing alumina content.

3.2. Residual stress determination

3.2.1. Piezospectroscopy results

The shifts of Cr^{3+} fluorescence spectra were measured for both the non-laminated alumina–zirconia mixture specimens and the outer compressive layer of the laminated specimens to determine the residual stress on the outer compressive layer. Figure 6a shows the residual stresses in the alumina grains in the non-laminated alumina–zirconia materials. As shown, the alumina grains were placed in compression due to the greater contraction of the zirconia grains during cooling. Also, as expected, the residual compressive stress in the alumina phase decreases with decreasing zirconia content.

Figure 6b shows the biaxial residual stress in the outer most compressive layers, based on the residual stresses in the un-laminated alumina–zirconia specimens shown in Fig. 6a. The residual compressive stresses measure with the piezospectroscopy method for the AZ50, AZ80, and AZ95 laminates are 675 ± 44 MPa, 1123 ± 60 MPa, and 1253 ± 79 MPa, respectively. The error bars show the standard deviation for at least five measurements for each composite.

3.2.2. Finite element analysis

The true specimen dimension FEA meshes were used, i. e. the meshes correspond to 425 μm thick zirconia layers, 60 μm thin compressive layers, and 45 μm out-most, thin, compressive surface layers. Due to the symmetry of the specimen, a mesh corresponding to 1/8 of the full specimen represented by gray lines in Fig. 7 was used. Residual stress determinations were made along the line 1, for the surface stress states, and the line 2, for interior stress states. Both σ_{xx} and σ_{zz} stress components were determined along these two lines.

Figure 8 shows the results of FEA for the AZ50 composite. In general and as expected, the interior biaxial stresses, σ_{zz} , shown in Fig. 8d, approximates a step function, with large compressive stresses within the thin layers and much smaller tensile stresses within the thick layers. The interior σ_{xx} stresses shown in Fig. 8c are different from expected values. Although the σ_{xx} stress (interior stress normal to the interfaces) are generally assumed to be zero, the FEA suggests they are finite, but very small with a maximum value at the center of the specimen approximately two orders of magnitude smaller than the interior biaxial, σ_{zz} stress.

Figure 8a shows the σ_{xx} stress at the surface showing that large tensile stresses exist on the surface of the thin layers, which, under the right conditions, produce edge cracking

[4]. According to the edge-cracking stress intensity function reported by Ho et al. [4], the analytical solution suggests that the maximum value of the surface tensile stresses should be equal to the absolute value of the interior compressive stresses. FEA results, Fig. 8a and Fig. 8d, indicate a good agreement with this analytical solution. There is a compressive stress component on the surface of thick tensile layers, i.e., the σ_{xx} surface stress shown at Fig. 8a. Figure 8b shows that the σ_{zz} stress at the surface is much smaller relative to the interior σ_{zz} stress states in Fig. 8d. It should be noted that the compressive σ_{zz} stresses are the ori-

gin of the crack arresting phenomenon. The biaxial compressive stress, σ_{zz} in Fig. 8d within the interior of the thin layers is about twice the value (~ 665 MPa), relative to the compressive surface stress σ_{zz} (~ 325 MPa) shown in Fig. 8b. Namely, the σ_{zz} stress on the surface is approximately 50% of those in the interior.

The FEA results for the AZ80 and AZ95 composites, shown in Fig. 9 and Fig. 10, illustrate the same relative results detailed for the AZ50 laminate, but with an increased magnitude of stress due to the larger differential thermal expansion difference for these composites.

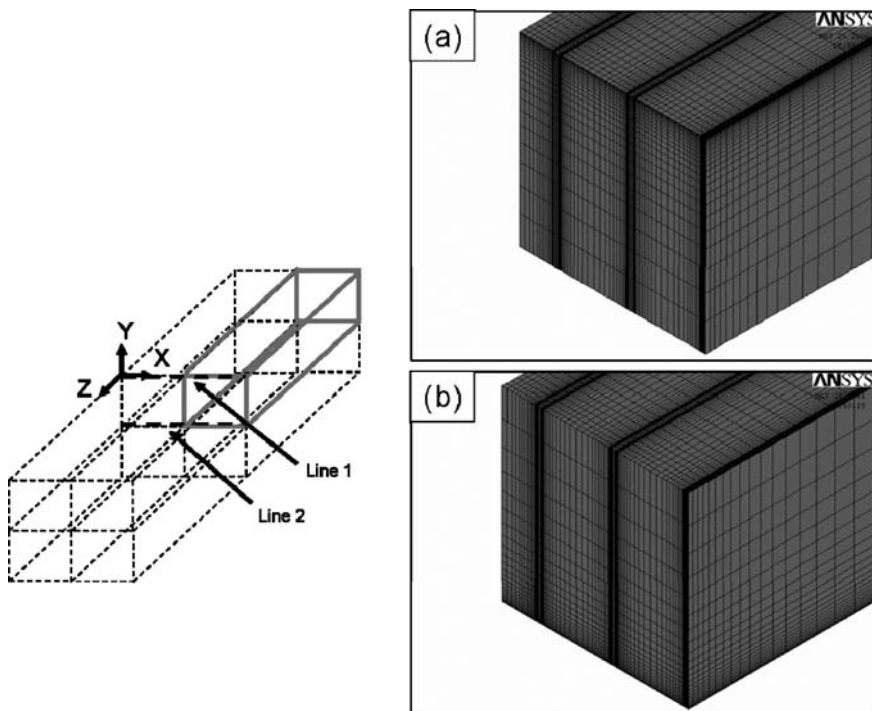


Fig. 7. The gray lines show the mesh used for the FEA model; specimen symmetry allowed modeling with only 1/8 of the real specimen size. The residual stresses were determined along the two dot-lines (surface stresses were calculated along line 1 and interior stresses were calculated along line 2) (a) FEA mesh for surface stress calculations along line 1; note the greater mesh density near the surface, relative to (b) FEA mesh used for the interior stress calculations along line 2.

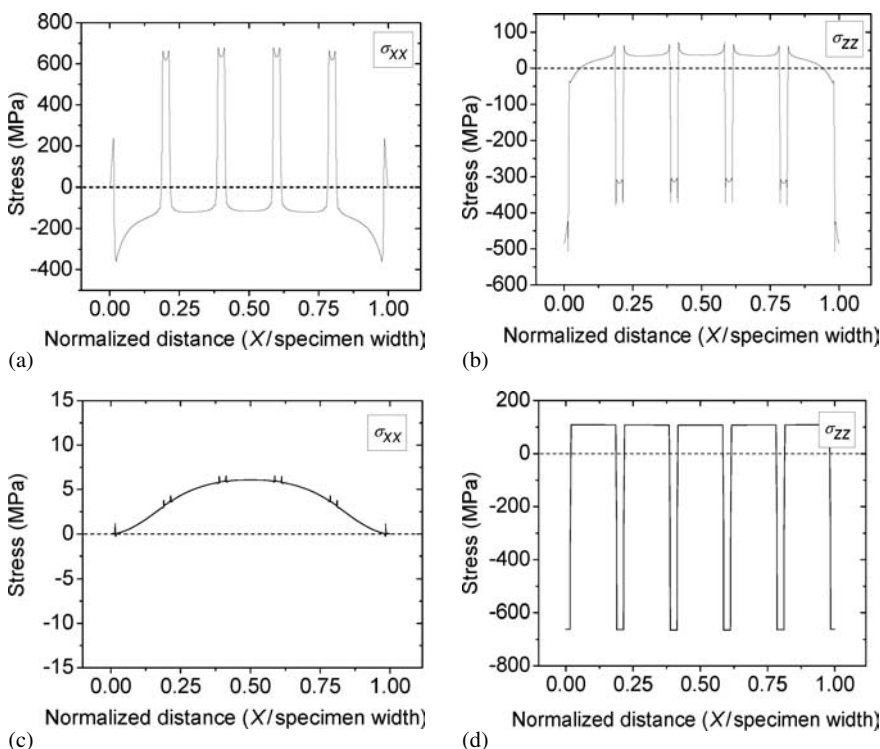


Fig. 8. FEA residual stress results for the AZ50 laminar composite. (a) and (b) show surface stresses calculated along the line 1 and (c) and (d) show interior stresses calculated along the line 2.

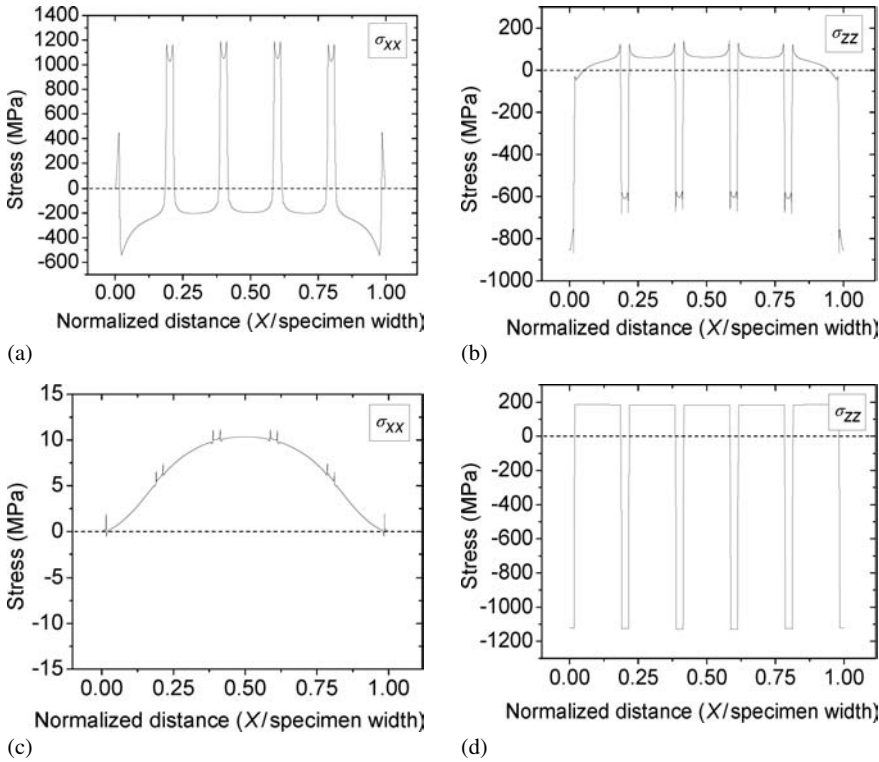


Fig. 9. FEA residual stress results for the AZ80 laminar composite. (a) and (b) show surface stresses calculated along line 1 and (c) and (d) show interior stresses calculated along line 2.

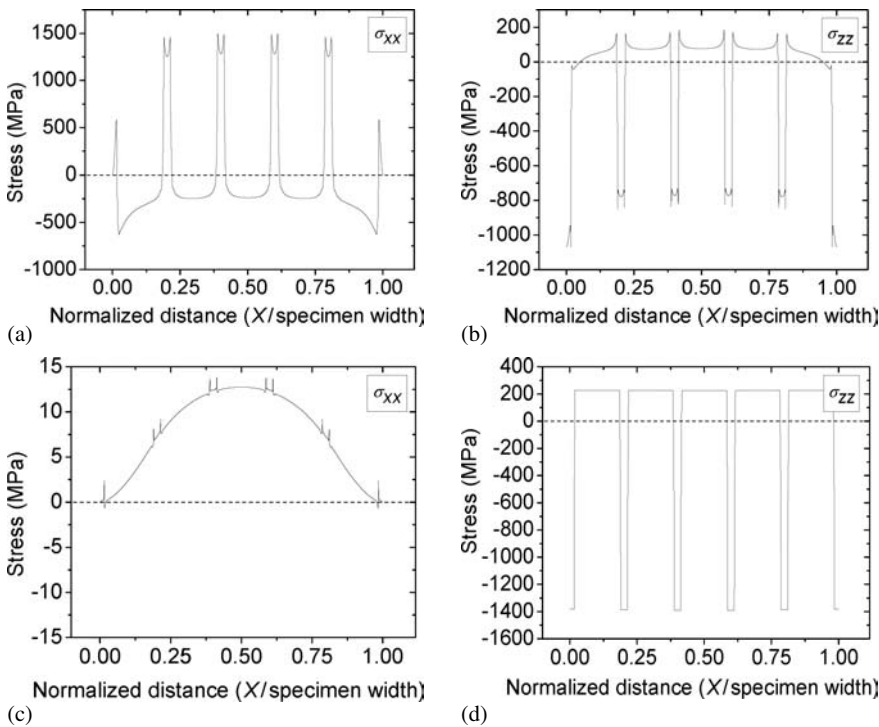


Fig. 10. FEA residual stress results for the AZ95 laminar composite. (a) and (b) show surface stresses calculated along line 1 and (c) and (d) show interior stresses calculated along line 2.

3.2.3. Indentation results

Figure 11a shows the crack produced with a Vickers indenter for an AZ80 specimen. It is obvious and expected that crack lengths are different because of the different stresses acting on the cracks described with the FEA results. As outlined above, by measuring the K_c and Vickers hardness of the zirconia material used to produce the thick layers, the residual stresses on the surface of the thick zirconia layers can be estimated using Eq. (7). The results are presented in Fig. 12. To avoid the influence of composite stresses, a

monolithic zirconia specimen was used to report the values for the hardness (HV) and K_c shown in Fig. 12a. These data were used to estimate the σ_{xx} and σ_{zz} surface stresses on the thick layer for the composite specimens reported in Fig. 12b and Fig. 12c, respectively.

3.2.4. Comparison of stresses

Residual stresses determined using the piezospectroscopy method, analytical method, and FEA are presented in Table 2. Table 3 shows residual stresses measured with inden-

© 2007 Carl Hanser Verlag, Munich, Germany www.ijmr.de Not for use in internet or intranet sites. Not for electronic distribution.

tation fracture methods and corresponding values from FEA results. Table 2 shows that piezospectroscopy, analytical, and FEA results are in good agreement.

Residual stress measurement results from indentation method and FEA show some agreements (see underlined data in Table 3). The deviations are not well understood but it appears that although the indentation method only

produces an approximate estimate of stress, the stress is in reasonable agreement with the FEA despite the large stress gradients associated with the surfaces. Notice that the results from indentation methods themselves show wide error bars and different results depending on the indenter loads used for the determination (see Fig. 12).

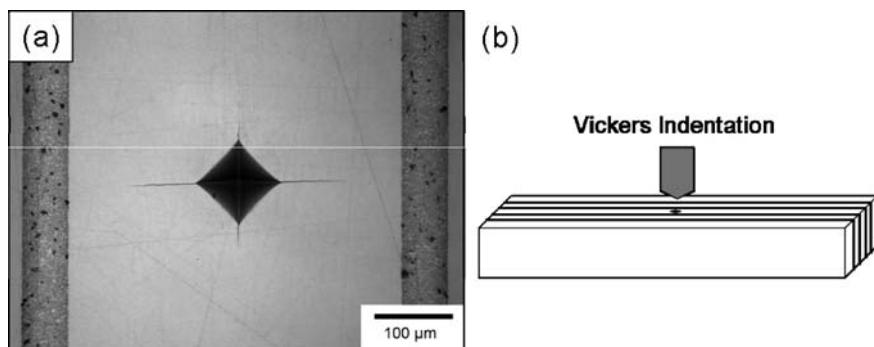


Fig. 11. Residual stress measurement using the indentation fracture method. (a) shows Vickers indented in an AZ80 specimen. The different crack lengths are due to the different residual stresses acting on the two perpendicular cracks. (b) shows schematic showing the configuration used to make Vickers indents.

Table 2. Interior residual stresses determined with the piezospectroscopy method, analytical method, and the Finite Element Analysis (FEA).

Specimen	Piezospectroscopy (Out-most Thin Layer)	Analytical (Interior)		FEA		
		Thin Layer σ_{zz} (MPa)	Thick Layer σ_{zz} (MPa)	(Out-most Thin Layer)	(Interior)	(Interior)
				σ_{zz} (MPa)	Thin Layer σ_{zz} (MPa)	Thick Layer σ_{zz} (MPa)
AZ50	-675 ± 44	-693.62	97.94	-662	-665	107
AZ80	-1124 ± 60	-1182.50	166.97	-1123	-1129	182
AZ95	-1226 ± 79	-1451.90	205.01	-1383	-1390	225

Table 3. Residual stresses on the surface of the thick layer estimated with the indentation fracture toughness method and compared to the FEA results. The underlined indentation stresses represent those in good agreement (within $\sim 10\%$) with stresses determined with the FEA method.

Specimen	Indentation Fracture Toughness (Surface Thick Layer)						FEA (Surface Thick Layer)	
	7 kg		9 kg		11 kg		σ_{xx} (MPa)	σ_{zz} (MPa)
	σ_{xx} (MPa)	σ_{zz} (MPa)	σ_{xx} (MPa)	σ_{zz} (MPa)	σ_{xx} (MPa)	σ_{zz} (MPa)		
AZ50	-186 ± 19	16 ± 9	<u>-105 ± 16</u>	<u>37 ± 2</u>	<u>-117 ± 24</u>	<u>37 ± 2</u>	-114	36
AZ80	-251 ± 12	44 ± 2	<u>-206 ± 15</u>	<u>54 ± 1</u>	<u>-215 ± 69</u>	<u>58 ± 6</u>	-194	62
AZ95	-357 ± 17	55 ± 2	<u>-240 ± 22</u>	<u>78 ± 8</u>	-308 ± 18	N/A	-239	76

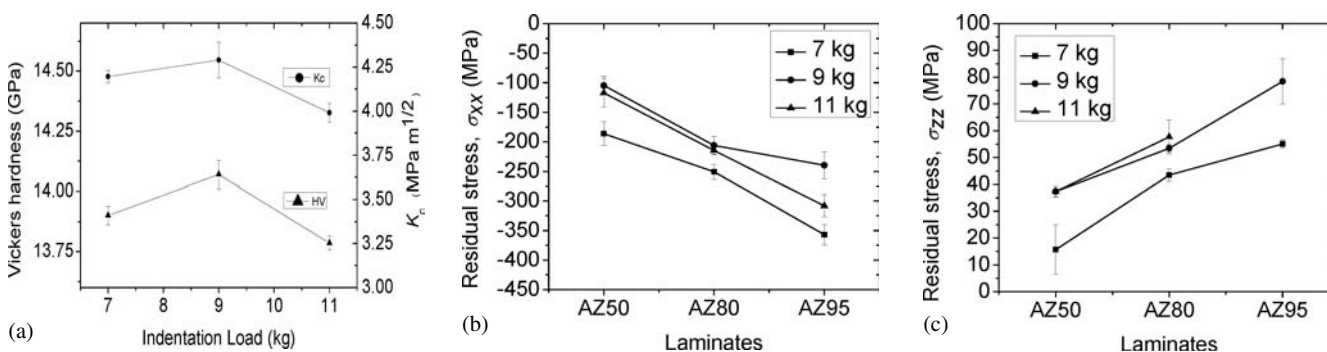


Fig. 12. (a) Hardness and K_c measurements as a function of indenter load. (b) and (c) Residual stresses measured using the indentation fracture method.

4. Discussion

Two factors, other than those expressed in Eq. (1), known to affect the threshold strength of the laminate have been reported. One is crack bifurcation [3] and the other is related to the elastic modulus ratio of the thin and thick layers [15]. Regarding crack bifurcation, when either the compressive stress or compressive layer thickness is large, the propagating crack will bifurcate within the compressive layer. Crack bifurcation is known to increase the threshold strength of the laminates, relative to the variables expressed in Eq. (1) [3]. When the elastic modulus ratio, E_1/E_2 , is greater than one, i.e., the modulus of the compressive layer is smaller than the tensile layer, it has been shown [15] that the applied stress intensity factor is smaller than that reported in Eq. (1), because of the lower strain energy density in the compressive layer [15, 16]. For the zirconia–alumina AZ50, AZ80, and AZ95 laminates studied here, the compressive layer has a higher elastic modulus relative to the thicker, zirconia layer, by factors of 1.42, 1.72, and 1.89, for the AZ50, AZ80 and AZ95 composites, respectively. Thus, due to the larger modulus of the compressive layers for composites studied here, the threshold strength would be expected to be smaller than expected from Eq. (1).

In the current study, a third factor was discovered that could influence the threshold strength. As shown in Figs. 8–10, the residual compressive stresses on the surface of the compressive layers are much smaller relative to those deep within the compressive layer. The compressive stresses deep within the compressive layer, which are usually calculated using Eq. (3), are generally used to estimate the threshold strength via Eq. (1). On the other hand, since the cracks that cause failure initiate at the surface (in the current experiments, though, the indentation crack), the much lower compressive stress at the surface, discovered though the FEA study, are expected to dramatically reduce the magnitude of the threshold strength, relative to that estimated using Eq. (1). Consequently, one would expect that both the lower compressive stresses at the surface, and the higher elastic modulus of the compressive layer reduced the threshold strength relative to those estimated using Eq. (1). This is exactly what was observed.

Four different methods were used to measure the residual stresses. Comparing the finite element results with the results from piezospectroscopy shows that piezospectroscopy, a simple method to use, produced accurate results. The indentation fracture toughness test is a very simple method, but although the agreement with FEA calculations is not as good as the piezospectroscopy results, it was better than initially expected. Larger indentation loads produced better agreement. Both the fracture toughness and Vickers hardness values were dependent on the indent load, more than likely due to the large amounts of plasticity that occur during the indentation of zirconia. The FEA method produced precise stress determination and produced a greater insight of the residual stresses in the laminate system. However users of FEA should be aware of the conditions of the modeling. For example, the stress release due to edge cracking was not considered in the FEA calculation, which should reduce a portion of the surface residual stress σ_{xx} for AZ80 and AZ95 laminates. Even though the edge crack was not considered in the model, one could obtain a good understanding of surface tensile stress that is the driving force of edge cracking.

5. Conclusions

Three different zirconia–alumina laminates, AZ50, AZ80, and AZ95, were fabricated via tape-casting $Zr(3Y)O_2$ thick layers, and dip-coating these thick layers with a mixture of zirconia and alumina, warm pressing and densification. The threshold strengths were determined to be 255 ± 8 MPa, 311 ± 7 MPa, and 421 ± 12 MPa for AZ50, AZ80, and AZ95 laminates, respectively, where the $Zr(3Y)O_2$ thick layers were $425 \mu m$ and thin layers $60 \sim 65 \mu m$. These values are about $60 \sim 70\%$ of those calculated from a previously reported function that would predict values of 413.82 MPa, 533.77 MPa, and 617.88 MPa for the same composites. It appears that the larger elastic modulus of the compressive layers, which contain alumina, and the much lower compressive stresses on the surface of the compressive layers, which were only evident in the FEA, produce the lower predicted threshold strength.

References

[1] M.P. Rao, A.J. Sanchez-Herencia, G.E. Beltz, R.M. McMeeking, F.F. Lange: Science 286 (1999) 102.
 [2] H. Moon, M.G. Pontin, F.F. Lange: J. Am. Ceram. Soc. 87 (2004) 1694.
 [3] M.P. Rao, F.F. Lange: J. Am. Ceram. Soc. 85 (2002) 1222.
 [4] S. Ho, C. Hillman, F.F. Lange, Z. Suo: J. Am. Ceram. Soc. 78 (1995) 2353.
 [5] M.G. Pontin, M.P. Rao, A.J. Sanchez-Herencia, F.F. Lange: J. Am. Ceram. Soc. 85 (2002) 3041.
 [6] S.F. Fillery, F.F. Lange: J. Am. Ceram. Soc. (in press).
 [7] Q. Ma, D.R. Clarke: J. Am. Ceram. Soc. 77 (1994) 298.
 [8] G.E. Fair, M.Y. He, R.M. McMeeking, F.F. Lange: J. Am. Ceram. Soc. 88 (2005) 1879.
 [9] V. Sergo, X.L. Wang, D.R. Clarke, P.E. Becher: J. Am. Ceram. Soc. 78 (1995) 2213.
 [10] F. Wakai, T. Nagono: J. Mat. Sci. Lett. 7 (1988) 607.
 [11] D.J. Green: An Introduction to the Mechanical Properties of Ceramics, Cambridge University Press, Cambridge (1998).
 [12] G.R. Anstis, P. Chantikul, B.R. Lawn, D.B. Marshall: J. Am. Ceram. Soc. 64 (1981) 533.
 [13] K.Y. Zeng, D. Rowcliffe: J. Am. Ceram. Soc. 77 (1994) 524.
 [14] D. Hull: Fractography: Observing, Measuring, and Interpreting Fracture Surface Topography, Cambridge University Press, Cambridge, UK, New York (1999).
 [15] K. Hbaieb, R.M. McMeeking: Mech. Mater. 34 (2002) 755.
 [16] M.G. Pontin, F.F. Lange: J. Am. Ceram. Soc. 88 (2005) 376.
 [17] A.J. Monkowski, G.E. Beltz: Int J. Solids Struct. 42 (2005) 581.

(Received January 25, 2007; accepted April 24, 2007)

Bibliography

DOI 10.3139/146.101522
 Int. J. Mat. Res. (formerly Z. Metallkd.)
 98 (2007) 8; page 674–682
 © Carl Hanser Verlag GmbH & Co. KG
 ISSN 1862-5282

Correspondence address

Fred F. Lang
 Materials Department
 University of California at Santa Barbara
 Santa Barbara, CA 93106, California, USA
 E-mail: flange@engineering.ucsb.edu

You will find the article and additional material by entering the document number MK101522 on our website at www.ijmr.de